# Capturing non-Markovian dynamics with the reaction coordinate method

Nicholas Anto-Sztrikacs[1] and Dvira Segal[2,1,*]

[1]*Department of Physics, 60 Saint George St., University of Toronto, Toronto, Ontario, Canada M5S 1A7*

[2]*Department of Chemistry and Centre for Quantum Information and Quantum Control, University of Toronto, 80 Saint George St., Toronto, Ontario, Canada M5S 3H6*

(Received 5 October 2021; accepted 9 November 2021; published 23 November 2021)

The reaction coordinate (RC) technique is emerging as a significant tool in the study of quantum dissipative dynamics and quantum thermodynamics. With the objective to further establish this tool, here we explore to what extent the method can capture non-Markovian dynamics of open quantum systems. As a case study, we focus on the pure decoherence model of a spin coupled to a harmonic reservoir. We compare the spin dynamics and measures for non-Markovianity from the exact analytical solution to simulations based on the RC method at the level of a second-order quantum master equation. We find that the RC method can quantitatively capture non-Markovian effects at strong system-bath coupling and for structured baths. This is rationalized by the fact that the collective RC bath mode, which is made part of the system, maintains system-bath correlations. Lastly, we apply our RC method and study the spin-boson model in the non-Markovian regime.

DOI: 10.1103/PhysRevA.104.052617

## I. INTRODUCTION

Quantum systems are never completely isolated from their surroundings, thus a build-up of system-bath correlations and the exchange of, e.g., particles, energy and information between the system and their environment is inevitable. Theoretical techniques that can faithfully capture these effects are required. This research area, traditionally developed to treat chemical problems in the condensed phases [1,2] and light-matter (quantum optics) problems [3] has been recently receiving much attention in relation to the field of quantum thermodynamics and more broadly quantum technologies [4].

Proposals to design quantum thermal machines that build on nontrivial quantum effects such as quantum coherences, correlations, and quantum statistics are analyzed with a range of open quantum system methods, particularly quantum master equations (QMEs). Such methods rely on two approximations to make the dynamics tractable: (i) Under the Born approximation one assumes that the system-reservoir coupling strength is weak, thus the dynamics can be solved to second order in the system-reservoir coupling parameter. This assumption results in ignoring the buildup of correlations between the system and its surroundings. (ii) QMEs such as the Redfield equation rely on the Markov approximation. This assumption concerns the lack of memory in the dynamics of the system, making it time-local, essentially ignoring any dynamical back flow from the reservoir to the system [1–3]. Although such second-order QME approaches yield accurate results within their regime of validity, they are quite restrictive and do not convey the correct dynamics when system and reservoirs influence each other's dynamics, as is the case of non-Markovian evolution [5–9].

Qualitatively, non-Markovian memory effects typically emerge at strong system-bath coupling and when the bath spectral density function is structured such that specific modes are more strongly coupled to the system. The unwritten rule is that non-Markovian dynamics demonstrate as recoherence effects and a departure from monotonic exponential decay.

The reaction coordinate mapping [10] seems well-suited to describe non-Markovian scenarios. This method, suggested in Refs. [11–13], redefines the system-environment boundary with the identification and extraction of a central (collective) degree of freedom of the environment, termed the reaction coordinate (RC). The quantum system is then extended to become a "supersystem," which comprises the original, premapped quantum system, the RC, and the interaction of the RC with the original system. For a schematic representation, see Fig. 1(a).

The advantage of the exact RC mapping becomes clear once we implement a second-order QME technique, such as the Born-Markov Redfield QME on the supersystem. The resulting technique, termed the RC-QME method, is nonperturbative in the original coupling parameter. Since the method enables cheap computations, it has been widely used in studies involving strongly coupled system-reservoirs. For example, it was utilized for studying the quantum dynamics of impurity models [14–16], thermal transport in nanojunctions [17,18], the operation of quantum thermal machines [19–21], and transport in electronic systems [22–24].

Earlier open-quantum-system methods were built on similar principles, treating non-Markovian baths by, e.g., extending the system or by building two-tiered environments (primary and secondary modes) and evolving dynamics with reduced equations of motion in the form of Langevin

*dvira.segal@utoronto.ca

 

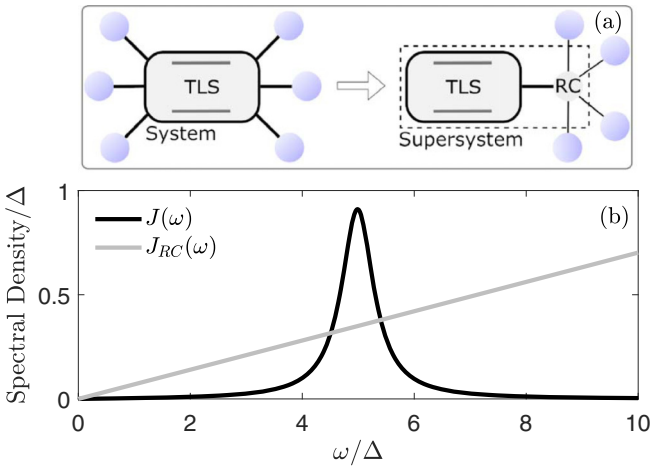


FIG. 1. (a) Representation of the RC transformation applied onto a two-level system coupled to a bosonic environment. (b) The Brownian spectral density function of the bath prior to mapping, $J(\omega)$, and postmapping, $J_{RC}(\omega)$, which is Ohmic. Parameters are $\Omega = 5$, $\gamma = 0.071$, $\lambda = 1.0$, $\Lambda = 1000\pi$, $\Delta = 1$.

[25], Fokker Planck [26], or master [27,28] equations; cited works are representative of a very rich literature. More recent works performed chain mapping [29,30] by iteratively adding bath modes to the system. Given recent studies of quantum transport and thermodynamics problems with the RC method, particularly for addressing system-bath coupling effects [16,18–21], here we focus on this specific formulation of nonperturbative open quantum system dynamics.

Due to the explicit inclusion of environmental degrees of freedom within the collective RC coordinate, it is expected that the RC-QME technique would properly capture non-Markovian effects. However, as of yet, no detailed study had attempted to address this issue using quantifiable non-Markovianity metrics, which is the objective of our work.

Quantification of non-Markovian dynamics has received ample attention in the last decade with various approaches suggested to define and compute it. Common measures of non-Markovianity are classified either as divisibility [31], or trace distance quantifiers [32]. The former defines a process as being non-Markovian if the quantum map of the open-system time evolution lacks the divisibility criterion stemming from the semigroup property. A trace distance quantifies the distinguishability of quantum states. Other measures proposed in the literature rely, for instance, on the quantum Fisher information [33], correlations [34,35], or, the volume of the Bloch sphere [36], to name a few. Comparative studies of different non-Markovianity metrics were given, e.g., in Refs. [37,38]. Beyond definitions and metrics, efficient computational methods have been developed to evaluate these measures, see, for example, Ref. [39], including machine learning techniques [40]. Many case studies of non-Markovian dynamics have dealt with a single qubit system [38,40] due to the difficulty in computing metrics of non-Markovianity. More complex models such as a pure decoherence model with a squeezed bath [41] or models of coupled qubits [42] have also been considered.

In this work, our objective is to assess the capability of the reaction coordinate technique in capturing non-Markovian dynamics. Towards this goal, we examine the exactly solvable pure decoherence model, which describes the phenomenon of phase loss between states building a quantum superposition. Studies of decoherence are central to understanding the quantum-to-classical crossover [43] and to the development of quantum computing devices [44]. Decoherence dynamics has been explored in experiments, see, e.g., Refs. [45–47]. Recent proposals suggest to employ it for pure-state thermometry [48]. Other recent studies examined corresponding heat transfer problems in the thermal bath [49,50].

We quantify non-Markovianity in the pure decoherence model using two well-studied methods: (i) The Breuer, Laine, and Piilo (BLP) measure, which concerns trace distance between states [32]. (ii) The Rivas, Huelga, Plenio (RHP) measure, which probes the complete positivity (CP) divisibility of the dynamical map [31].

By comparing the decoherence dynamics and measures for non-Markovianity from RC-QME simulations to exact expressions, we can appraise the RC-QME method, indeed judging it to excellently detail non-Markovian effects in time evolution.

The paper is organized as follows: In Sec. II, we introduce the pure decoherence model and the reaction coordinate mapping. The RC-QME method is presented in Sec. III. Measures for non-Markovianity are discussed in Sec. IV, with simulations presented in Sec. V. We discuss non-Markovianity in the more complex dissipative spin-boson model in Sec. VI, then conclude our work.

## II. PURE DECOHERENCE MODEL

We begin with the pure decoherence Hamiltonian [2,3],

$$\hat{H} = \frac{\Delta}{2}\hat{\sigma}_z + \hat{\sigma}_z \sum_k f_k(\hat{c}_k^\dagger + \hat{c}_k) + \sum_k \nu_k \hat{c}_k^\dagger \hat{c}_k. \tag{1}$$

Here, $\Delta$ is the energy splitting of the spin, $\hat{\sigma}_{x,y,z}$ are the Pauli matrices, $\hat{c}_k^\dagger$ ($\hat{c}_k$) are bosonic creation (annihilation) operators of the reservoir for a mode of frequency $\nu_k$. The bath's harmonic oscillators are coupled to the spin polarization with strength $f_k$. The effects of these interactions are captured by a spectral density function, $J(\omega) = \sum_k f_k^2 \delta(\omega - \nu_k)$. Since the system's Hamiltonian and its interaction with the bath commute, the system does not exchange energy with the bath.

Our objective is to focus on the non-Markovian dynamics of the spin. We amplify such non-Markovian evolution by choosing the spectral density function of the environment to be a Brownian function, peaked around a central mode $\Omega$ with a width parameter $\gamma$ and system-bath coupling strength $\lambda$ [51],

$$J(\omega) = \frac{4\omega\Omega^2\lambda^2\gamma/\pi}{(\omega^2 - \Omega^2)^2 + (2\gamma\Omega\omega)^2}. \tag{2}$$

Technically, this spectral function arises naturally in the derivation of the reaction coordinate mapping when one works backwards, first defining an Ohmic spectral function for the residual bath after the mapping [14].

Following a procedure analogous to that described in Refs. [14,18], we map the pure decoherence Hamiltonian, Eq. (1) using the reaction coordinate transformation. This mapping consists of preparing a collective coordinate of the environment, called the reaction coordinate (RC), and redefining the boundary between the system and the reservoir to include this coordinate as part of the system. Post-mapping, the physical picture consists of a spin coupled to the RC, which in turn couples to a residual harmonic reservoir. The reaction coordinate is a harmonic-bosonic mode with creation (annihilation) operator $a^\dagger$ ($a$). It is defined such that

$$\lambda(\hat{a}+\hat{a}^\dagger)=\sum_k f_k(\hat{c}_k+\hat{c}_k^\dagger). \tag{3}$$

This process results in the RC pure decoherence Hamiltonian,

$$\hat{H}_{\mathrm{RC}}=\hat{H}_{\mathrm{ES}}+\hat{H}_{\mathrm{B}}+\hat{H}_{\mathrm{ES,B}}. \tag{4}$$

It includes an extended system $\hat{H}_{\mathrm{ES}}$, a residual bath $\hat{H}_{\mathrm{B}}$, and their interaction $\hat{H}_{\mathrm{ES,B}}$,

$$\begin{aligned}\hat{H}_{\mathrm{ES}}&=\frac{\Delta}{2}\hat{\sigma}_z+\lambda\hat{\sigma}_z(\hat{a}^\dagger+\hat{a})+\Omega\hat{a}^\dagger\hat{a},\\ \hat{H}_B&=\sum_k\omega_k\hat{b}_k^\dagger\hat{b}_k,\\ \hat{H}_{\mathrm{ES,B}}&=(\hat{a}^\dagger+\hat{a})\sum_k g_k(\hat{b}_k^\dagger+\hat{b}_k)+(\hat{a}^\dagger+\hat{a})^2\sum_k\frac{g_k^2}{\omega_k}.\end{aligned} \tag{5}$$

Here, $\hat{b}_k^\dagger$ ($b_k$) are the creation (annihilation) operators of the residual bath, and $\Omega$ and $\omega_k$ are the frequencies of the RC and modes of the reservoir, respectively. The energy $\lambda$ corresponds to the coupling strength between the spin and the RC, while $g_k$ characterizes the coupling between the RC and the residual environment. This system-reservoir coupling (first term in $\hat{H}_{\mathrm{ES,B}}$) is described by the residual environment's spectral density, $J_{\mathrm{RC}}(\omega)=\sum_k g_k^2\delta(\omega-\omega_k)$. In correspondence with Eq. (2), we set this function to be Ohmic,

$$J_{\mathrm{RC}}(\omega)=\frac{\gamma}{\pi}\omega e^{-\omega/\Lambda}. \tag{6}$$

Here, $\gamma$ is a dimensionless parameter that captures the coupling strength between the residual bath and the extended system, $\Lambda$ is a high-frequency cutoff. In Fig. 1(b) we display the spectral density functions of the bath before and after the RC mapping.

By deriving equations of motion for operators in Eq. (5), it can be shown that in the limit of an infinite cutoff, the corresponding spectral function for the original reservoir is of a Brownian form, as depicted in Eq. (2). We emphasize that the mapping is exact and no approximations have been made so far to obtain the RC pure decoherence Hamiltonian, Eq. (5).

As a reminder, the pure decoherence model does not permit energy transport between the system and the environment, and it only allows the loss of quantum coherence in the system. This is because the system's Hamiltonian commutes with the total Hamiltonian: In the original picture, Eq. (1), both system and system-bath coupling operators align with $\hat{\sigma}_z$. In contrast, after the RC mapping the extended model obeys $[\hat{H}_{\mathrm{ES}},\hat{H}_{\mathrm{B}}+\hat{H}_{\mathrm{ES,B}}]\neq 0$.

Given its relative simplicity, it is possible to obtain an exact analytic solution to the decohering dynamics of Eq. (1) [1–3]. Namely, given an initial state for the system (after tracing out the bath),

$$\rho(0)=\begin{pmatrix}\rho_{00} & \rho_{01}\\ \rho_{10} & \rho_{11}\end{pmatrix},$$

it can be shown that, at a later time $t$, the state of the system evolves to

$$\rho(t)=\begin{pmatrix}\rho_{00} & \rho_{01}e^{\Gamma(t)-i\Delta t}\\ \rho_{10}e^{\Gamma(t)+i\Delta t} & \rho_{11}\end{pmatrix}. \tag{7}$$

While populations are constant in time, coherences can show nontrivial decaying dynamics. This behavior is captured via the decoherence function (we set Planck's and Boltzmann's constants to $\hbar\equiv 1$, $k_{\mathrm{B}}\equiv 1$),

$$\Gamma(t)=-4\int_0^\infty J(\omega)\coth\left(\frac{\beta\omega}{2}\right)\frac{1-\cos(\omega t)}{\omega^2}d\omega, \tag{8}$$

where $\beta$ is the inverse temperature of the bosonic reservoir. In Appendix A we show that, in the long-time limit and for nonzero temperature, the decoherence function reduces to

$$\Gamma(t)\xrightarrow{\text{long time}}-\frac{16\gamma\lambda^2}{\Omega^2\beta}t. \tag{9}$$

According to this result, coherences decay exponentially with time, with the decoherence timescale

$$\tau_D=\frac{\beta\Omega^2}{16\gamma\lambda^2}. \tag{10}$$

As we show in Appendix A, this result can be obtained directly from the exact expression, Eq. (8), as well as from the Redfield equation, which is built on the Born-Markov approximation.

## III. THE REACTION COORDINATE QUANTUM MASTER EQUATION METHOD

The simplicity of reaction-coordinate simulations stems from the fact that, once the RC is extracted from the environment and added to the system, we can employ standard Markovian weak-coupling quantum master-equation techniques to describe the dynamics of the supersystem; we use the Redfield equation. We refer to this approach, of extracting a RC from the bath then simulating the dynamics of the supersystem with the Redfield equation as the RC-QME method. In this section, we briefly describe this method and its implementation on the decoherence model.

We truncate the RC harmonic mode (eigenstates $|n\rangle$) to include $M$ energy levels; in simulations, $M$ should be taken sufficiently large to ensure convergence of results. The supersystem now includes a spin coupled to an $M$-level system, in turn coupled to a residual heat bath. The Hamiltonian is $\hat{H}_{\mathrm{RC}}^M=\hat{H}_{\mathrm{ES}}^M+\hat{H}_{\mathrm{ES,B}}^M+\hat{H}_{\mathrm{B}}$, corresponding to Eq. (4),

with

$$\hat{H}^M_{\rm ES} = \frac{\Delta}{2}\hat{\sigma}_z + \Omega\sum_{n=0}^{M-1}\left(\frac{1}{2}+n\right)|n\rangle\langle n| + \lambda\hat{\sigma}_z\sum_{n=1}^{M-1}\sqrt{n}(|n\rangle\langle n-1| + |n-1\rangle\langle n|),$$
$$\hat{H}^M_{\rm ES,B} = \sum_k\sum_{n=1}^{M-1}\sqrt{n}(|n\rangle\langle n-1| + |n-1\rangle\langle n|)g_k(\hat{b}_k + \hat{b}^\dagger_k). \tag{11}$$

In the last line, we neglected the nontrivial quadratic term: Once performing the Redfield QME, its impact is absorbed in the dissipator [14]. We can compactify the system-bath interaction as $\hat{H}^M_{\rm ES,B} = \hat{S}^M_{\rm ES}\otimes\hat{B}$, identifying $\hat{S}^M_{\rm ES}$ and $\hat{B}$ from Eq. (11). Note that $\hat{S}^M_{\rm ES}$ is defined in the $2M$-dimensional Hilbert space of the supersystem.

To study dynamics and steady-state values, we employ the energy-basis Redfield QME. As such, we first diagonalize $\hat{H}^M_{\rm ES}$ in Eq. (11) with a unitary operator $\hat{U}$, a process that we do numerically. The transformed supersystem operators are $\hat{H}^D_{\rm ES} = \hat{U}^\dagger\hat{H}^M_{\rm ES}\hat{U}$, $\hat{S}^D_{\rm ES} = \hat{U}^\dagger\hat{S}^M_{\rm ES}\hat{U}$.

The Redfield equation is reliable for our model as long as (i) the coupling energy of the extended system to the residual bath is small. In terms of model parameters, this means that $\gamma\Delta \ll T$. This assumption is necessary for the second-order perturbative treatment of the RC quantum master equation to yield accurate results. (ii) The residual reservoir should be relatively structureless, supporting a Markov approximation on the supersystem. (iii) As an initial condition, the total state is assumed factorized into the supersystem times bath states. Furthermore, the state of the reservoir is given by a canonical thermal state at temperature $T = 1/\beta$.

In the Schrödinger picture, the Redfield time evolution of the extended system is given by

$$\dot{\rho}_{\rm ES}(t) = \mathcal{L}_{\rm red}\rho_{\rm ES}(t) = -i\big[\hat{H}^D_{\rm ES}, \rho_{\rm ES}\big] + D(\rho_{\rm ES}), \tag{12}$$

with the Liouvillian $\mathcal{L}_{\rm red}$ including the unitary dynamics and the Redfield dissipator $D$. For completeness, these expressions are included in Appendix B.

We time-evolve the dynamics subject to initial coherences. However, since we are not interested in the dynamics of the reaction coordinate itself—but the spin alone—we trace out the RC degree of freedom,

$$\rho(t) = {\rm Tr}_{\rm RC}[e^{\mathcal{L}_{\rm red}t}\rho_{\rm ES}(0)]. \tag{13}$$

As for the initial condition of the supersystem $\rho_{\rm ES}(0)$ we assume that the spin and the RC are prepared in a product state, $\rho_{\rm ES}(0) = \rho(0)\otimes\rho_{\rm RC}(0)$, with the RC initially thermalized to the attached reservoir. Therefore, ignoring the zero-point energy (which is not influential here) we write $\rho_{\rm RC}(0) = \frac{e^{-\beta\Omega a^\dagger a}}{Z}$, with $Z = {\rm Tr}_{\rm RC}[e^{-\beta\Omega a^\dagger a}]$ being the partition function of the reaction coordinate. Note that, in the truncated basis, we normalize level populations to unity. The initial state of the spin is ours to choose. For the purpose of decoherence dynamics explorations we arbitrarily set it to be $\rho(0) = \frac{1}{2}(|0\rangle + |1\rangle)(\langle 0| + \langle 1|)$.

The RC-QME time evolution, Eq. (13), is nonperturbative in $\lambda$, the original system-bath coupling energy. It is perturbative, however, in the width parameter $\gamma$ because we invoke the Born-Markov approximation on the extended model. Given that the RC is embedded in this model, we expect non-Markovian effects to be preserved in the dynamics. To quantify the extent of non-Markovianity captured by the RC-QME method we benchmark it against exact results based on the decoherence function, Eq. (8). We further compare the RC-QME technique to the standard Born-Markov-Redfield quantum master equation (BMR-QME) on the original model without the extraction of the RC. This method handles system-bath couplings $\lambda$ to second order only.

## IV. MEASURES OF NON-MARKOVIANITY

Unlike classical Markovian dynamics, which is mathematically well-defined using classical stochastic processes, quantum Markovianity is nontrivial to quantitatively define, and the literature includes numerous definitions and metrics to quantify it [3,5,6,8,9]. Many of these measures can be arranged into two classes, concerning (i) the distinguishability of states and (ii) divisibility of the dynamical map. Underlying such measures are concepts such as trace distance, fidelity, negativity of the decay rate, system-bath correlations and information flow [5]. Despite their differences, a unifying aspect concerning measures for non-Markovianity is the emergence of memory effects within the open quantum system dynamics often visible with recoherences.

In this work, we do not aim to adjudicate between different quantifiers for non-Markovianity. With the objective to assess to what extent the RC-QME method can capture non-Markovian dynamics, we employ two distinct, well-accepted quantifiers for non-Markovianity: The BLP [32] measure on the distinguishability of states, and the RHP quantifier [31] on the complete positive (CP) divisibility of the dynamical map. With extensive simulations and benchmarking against exact results, we demonstrate that the RC-QME technique excellently captures non-Markovian dynamics in the pure decoherence model.

### A. Breuer, Laine, Piilo Measure

In their influential work, Breuer, Laine, and Piilo presented the so-called BLP measure for non-Markovianity [32]. This metric is based on the nonmonotonicity of the trace distance $D$ between quantum states,

$$D(\rho_1,\rho_2) = \tfrac{1}{2}||\rho_1 - \rho_2|| = \tfrac{1}{2}\sum_i|\epsilon_i|. \tag{14}$$

Here, $\rho_1$ and $\rho_2$ are two quantum states, and $\epsilon_i$ are the eigenvalues of the Hermitian operator $\rho_1 - \rho_2$. The trace distance can be interpreted as a measure for state distinguishability: It returns values between 0 and 1, ranging from indistinguishable (0) to distinguishable (1) states. A decrease in trace distance is associated with a reduced ability to distinguish between two states. In our context, this is associated with a loss of information over the quantum system. Conversely, an

increase in the trace distance corresponds to a higher ability to distinguish states, interpreted as information returning to the open system from the reservoir. This situation can be attributed to the survival of memory effects in the dynamics.

To quantify non-Markovianity, one adds contributions of the trace distance in regions where it is increasing,

$$\mathcal{N}_{\mathrm{BLP}} = \max_{\rho_1,\rho_2} \int_{\sigma>0} dt\sigma(t,\rho_1,\rho_2). \tag{15}$$

Here $\sigma(t,\rho_1,\rho_2) = \frac{d}{dt}D(\rho_1(t),\rho_2(t))$, where $\rho_1$ and $\rho_2$ are the initial states and $\rho_1(t)$ and $\rho_2(t)$ are time evolved states under a certain dynamical equation. Note that the measure is obtained after maximization over all pairs of initial states; it has been shown that the pair of states that maximize the BLP measure, Eq. (15), are orthogonal. Furthermore, it can be shown that the trace distance is contractive for any completely positive trace-preserving map.

Equation (15) is not fully transparent, and the required optimization can make it a heavy task to compute [32]. Luckily, for the exactly solvable decoherence model the states maximizing the increase of the trace distance can be identified. Thus, an analytic expression can be derived for the BLP measure. It is given in terms of the decoherence function, Eq. (8), as [37,39]

$$\mathcal{N}_{\mathrm{BLP}} = \sum_j [e^{\Gamma(b_j)} - e^{\Gamma(a_j)}]. \tag{16}$$

Here, $t \in [a_j, b_j]$ indicates the $j$th time interval in which the trace distance is increasing. For a Markovian process, the non-Markovianity measure is zero.

### B. Rivas, Huelga, Plenio Measure

The Rivas, Huelga, Plenio measure for non-Markovianity inquires on the CP-divisibility property of the dynamical map [31]. Considering a QME of Lindblad form with a set of time-dependent rates $\gamma_k(t)$, divisibility, and thus Markovianity, is identified if the rates are positive throughout, $\gamma_k(t) \geqslant 0$. Namely, according to the RHP measure, a dynamical process is Markovian if the dynamical map can be split (factorized) at all times. A process evolves under non-Markovian dynamics if there is a lack of divisibility. Concretely for the pure decoherence model the RHP measure is given by [37]

$$\mathcal{N}_{\mathrm{RHP}} = \sum_j [\Gamma(b_j) - \Gamma(a_j)], \tag{17}$$

where similarly to before, $t \in [a_j, b_j]$ is the $j$th interval where nonmonotonic decay takes place. In contrast with the BLP measure, this quantifier does not require optimization, therefore, it is generally easier to compute than the BLP.

We evaluate Eqs. (16) and (17) in two ways: (i) by using the exact analytic form, Eq. (8), and (ii) approximately, by simulating the dynamics with the RC-QME method as described in Sec. III. In the latter case, we time-evolve an initial state of the system to long-enough times according to Eq. (13), then evaluate the decoherence function from the ratio $e^{\Gamma_{\mathrm{RC}}(t)} \equiv |\rho_{01}(t)/\rho_{01}(0)|$.

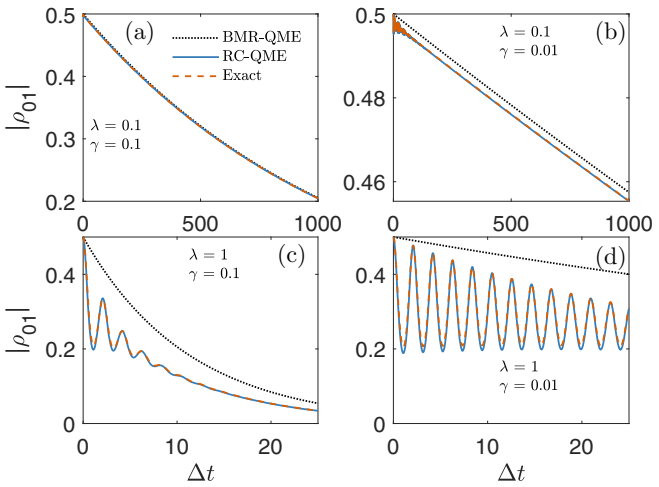


FIG. 2. Decoherence dynamics with bath structuring (small $\gamma$) and enhanced coupling (large $\lambda$). We display coherences $|\rho_{01}|$ starting from $\rho_{01}(t=0) = 1/2$ as a function of the dimensionless time $\Delta t$ using the Born-Markov Redfield QME (dotted) the RC-QME method (full), and the exact analytical solution (dashed). Parameters are $\Delta = 1$, $\Omega = 3$, $T = 0.5$, $\Lambda = 1000\pi$, and $M = 8$. Note that all parameters are given in units of $\Delta$.

## V. RESULTS

We study the dynamics of the decoherence model, Eq. (1), with (i) the exact expression (Exact) Eq. (8), (ii) the reaction-coordinate method (RC-QME), and (iii) the Born-Markov Redfield approach without the RC mapping (BMR-QME). We emphasize that the BMR-QME is perturbative in the coupling energy $\lambda$, while the RC-QME treats $\lambda$ to all orders and is instead perturbative in the width parameter $\gamma$. As such, for weak and intermediate couplings, the RC-QME very well performs against exact results. We further illustrate its challenges at strong couplings: Once $\lambda \gtrsim \Omega$, the RC-QME method poorly converges with the number of levels, $M$. Beyond studies of dynamics, we use the BLP and the RHP metrics to quantify non-Markovianity in the pure decoherence model comparing results from the exact decoherence function to RC-QME simulations.

### A. Decoherence dynamics

We examine the role of the system-bath coupling $\lambda$ and the bath structuring parameter $\gamma$ on $\rho_{01}(t)$ in Fig. 2. By comparing RC-QME simulations (full) to the exact expression (dashed) we conclude that the RC-QME accurately captures the dynamics at both short and long times and from small to large $\gamma$ and $\lambda$. In contrast, the BMR-QME method (dotted) fails to follow the correct dynamics of $\rho_{01}(t)$ at large $\lambda$ and small $\gamma$.

Since the BMR-QME method only describes Markovian dynamics with an exponential decay of coherences (see Appendix A), we conclude, qualitatively at this point, that the RC-QME method properly describes non-Markovian effects, roughly identified here by recoherences. Next, we discuss in more details the role of $\lambda$ and $\gamma$ in the decoherence dynamics.

*Structuring of the bath.* Small width parameter $\gamma$ corresponds to a sharp spectral density function of the thermal bath, which is commonly associated with the emergence of

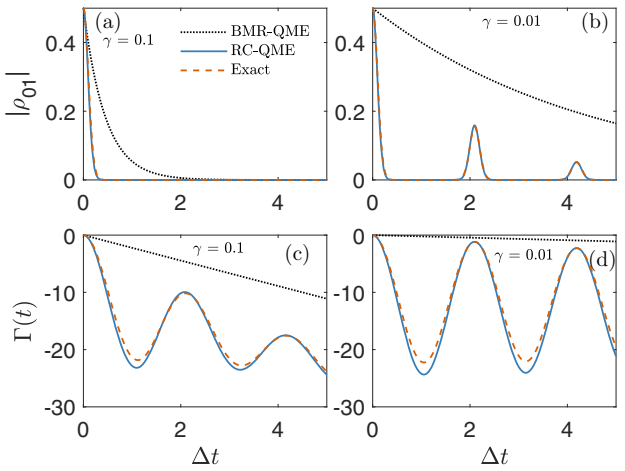


FIG. 3. Recoherence behavior at strong coupling, $\lambda = 5$. Starting from $\rho_{01} = 1/2$ we present (a), (b) the dynamics of $|\rho_{01}(t)|$ and (c), (d) the decoherence function. Parameters are the same as in Fig. 2 with the BMR-QME (dotted), the RC-QME with $M = 50$, (full), and the exact analytical solution (dashed).

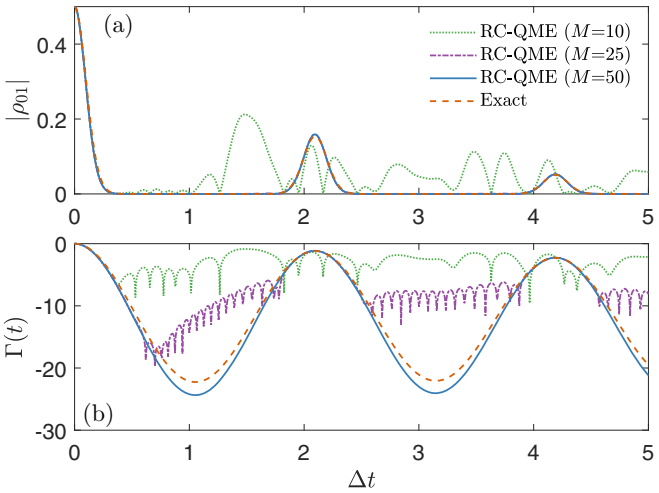


FIG. 4. Convergence of the RC-QME simulations, Figs. 3(b) and 3(d), with respect to $M$ at strong coupling, $\lambda = 5$. We present the (a) decoherence dynamics and (b) decoherence function for $M = 10$ (dotted), 25 (dashed-dotted), 50 (full), and compare those to exact results (dashed).

non-Markovian dynamics. Indeed, as we reduce $\gamma$ we observe deviations from the Markovian-exponential trend, compare Fig. 2(a) with Fig. 2(b) and Fig. 2(c) with Fig. 2(d). Recoherence dynamics is most pronounced in Fig. 2(d) at strong coupling and for small width $\gamma$.

*System-bath coupling.* We pinpoint the impact of $\lambda$ on the decoherence timescale by comparing Fig. 2(a) with Fig. 2(c). As expected, this timescale is shorter at strong coupling in accord with Eq. (8), $\Gamma(t) \propto \lambda^2$. The same conclusion is arrived at when comparing Fig. 2(b) with Fig. 2(d). Note on the different timescales presented in these different panels: The decoherence characteristic time is $\tau_D = \frac{\beta\Omega^2}{16\gamma\lambda^2}$, resulting in $\tau_D \approx 1.13\times10^4$ and $1.13\times10^2$ in Figs. 2(b) and 2(d), respectively. Thus, we expect to see significant suppression of coherences around those timescales.

We focus on the strong-coupling behavior in Fig. 3 and present results in both the large-$\gamma$ region [Figs. 3(a) and 3(c)] and highly non-Markovian (small $\gamma$) regime [Figs. 3(b) and 3(d)]. We note on the accuracy of the RC-QME method in capturing decoherence dynamics, as compared with exact results, in contrast with the complete failure of the BMR-QME method. This agreement is notable given dramatic recoherence dynamics observed at small $\gamma$ in Fig. 3(b). When inspecting the decoherence function in Fig. 3(c), we observe oscillatory dynamics, the expected signature of non-Markovianity. Yet, this rich dynamics does not show up in Fig. 3(a), where the magnitude of coherences appears to be monotonically decreasing with no features. However, we note that the scale of the $y$ axis in Fig. 3(c) is rather small; recall that $|\rho_{01}(t)| = |\rho_{01}(0)|e^{\Gamma(t)}$, thus having little impact on the magnitude of coherences.

*Convergence.* RC-QME simulations should be converged with respect to $M$, the number of levels representing the RC harmonic oscillator. Simulations in Fig. 2 at small to intermediate $\lambda$ excellently converge with $M = 8$, see Appendix D. In contrast, converging the large-$\lambda$ dynamics presented in Fig. 3 requires a large number of RC levels, up to $M = 50$. Thus, the RC-QME method becomes impractical to use at strong coupling, $\lambda \gtrsim \Omega$, and small $\gamma$ because it scales unfavorably with $M$.

To illustrate the difficulty in converging RC-QME simulations at large $\lambda$, in Fig. 4 we display the decoherence dynamics for three different $M$ values: 10, 25, and 50. Comparing their behavior in Fig. 4(a) we notice that $M = 10$ completely misses the dynamics by many orders of magnitude. Furthermore, according to Fig. 4(a), $M = 25$ seemingly agrees with exact results. However, a careful inspection of the decoherence function itself in Fig. 4(b) reveals significant deviations. It is only at large $M$, here at $M = 50$, that results converge and further reasonably agree with exact results.

Interestingly, Fig. 4 reveals another aspect of the RC-QME method: It tends to overestimate the effect of non-Markovianity. Staying with a qualitative picture for now, we identify non-Markovianity in our model with the departure from an exponential decay and appearance of recoherences [52,53]. Figure 4(b) reveals that the RC technique displays deeper troughs than exact results. This points to the fact that the inclusion of one specific RC mode into the system may lead to an overestimation of non-Markovian features.

### B. Quantifying non-Markovianity

We quantify the degree of non-Markovianity in the dynamics using the different measures focusing on the performance of the RC-QME method compared with the exact expression. We adopt the BLP measure for non-Markovianity in Fig. 5 and the RHP quantifier in Fig. 6, examining their dependence on the system-bath coupling $\lambda$ and the spectral width $\gamma$. Each data point in Figs. 5 and 6 was obtained by processing long time traces of decoherence dynamics using the quantifiers, Eqs. (15) and (17). Time traces extend from initial conditions at $t_i$ to a long time $t_f$ at which recoherences become insignificant. These figures thus compile significant data; while convergence was rapid for small $\lambda$ [Figs. 5(c) and 6(c)]. It was

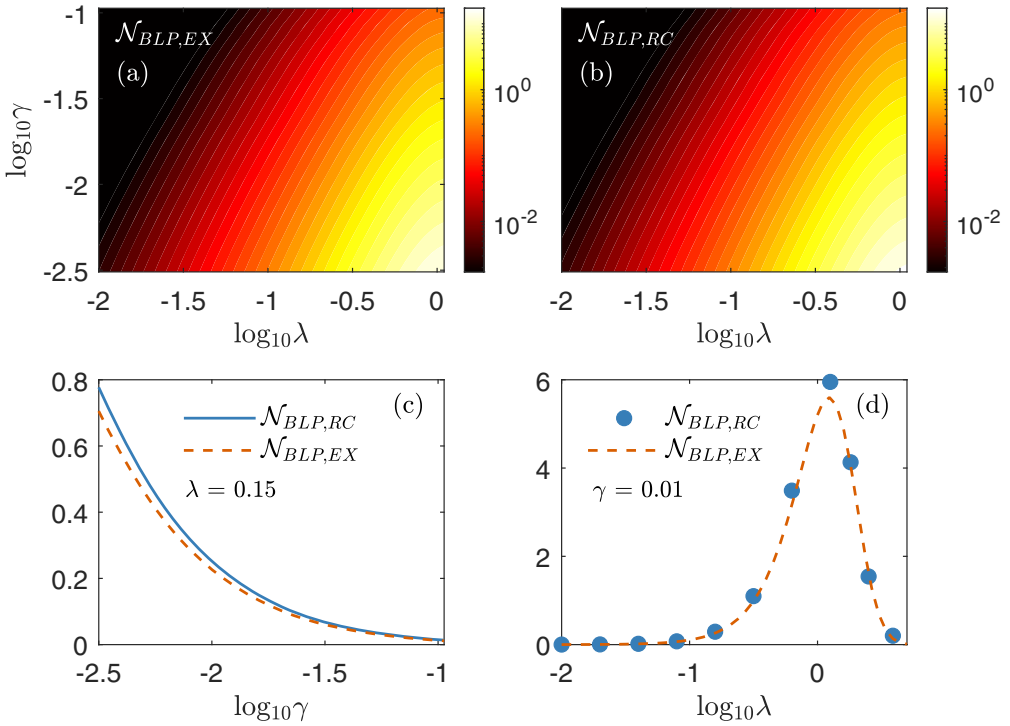


FIG. 5. The BLP measure of non-Markovianity as a function of the coupling energy $\lambda$ and spectral density width $\gamma$. We present contour maps based on (a) the exact dynamics and (b) RC-QME simulations. We further show the BLP measure (c) as a function of $\gamma$ at weak coupling (we used $M = 8$) and (d) as a function of $\lambda$ for small $\gamma$ (with $M = 50$) using the exact expression (dashed) and RC-QME simulations (full or circles). Parameters are the same as in Fig. 2.

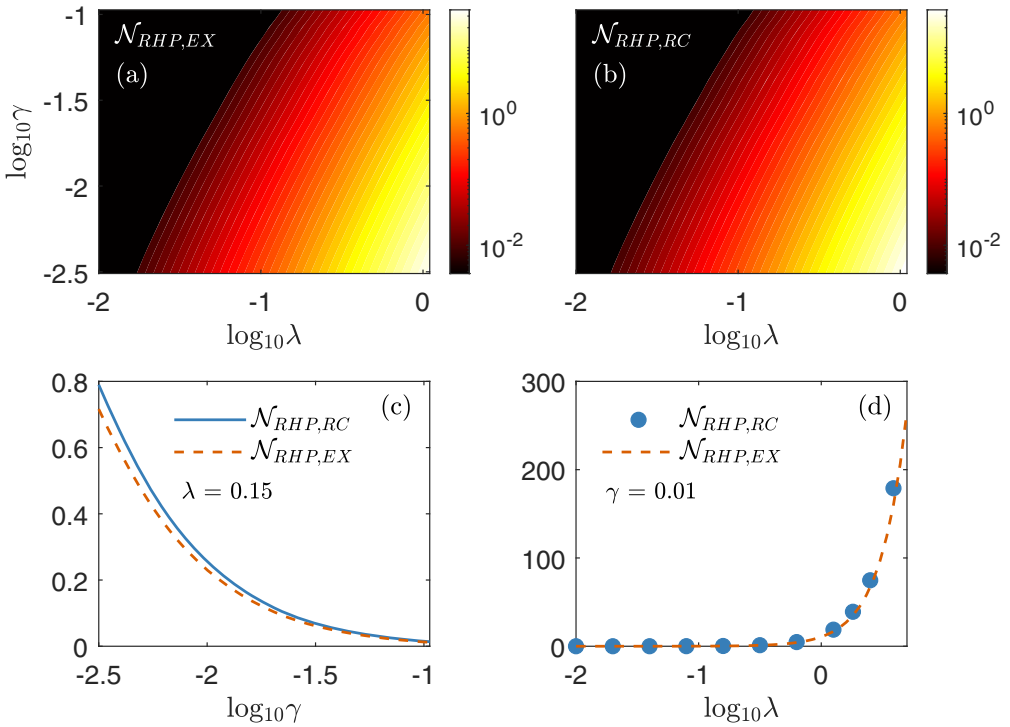


FIG. 6. The RHP measure of non-Markovianity as a function of the coupling energy $\lambda$ and spectral density width $\gamma$. We present contour maps based on (a) the exact dynamics and (b) RC-QME simulations. We further show the RHP measure (c) as a function of $\gamma$ at weak coupling (we used $M = 8$) and (d) as a function of $\lambda$ for small $\gamma$ (with $M = 50$) using the exact expression (dashed) and RC-QME simulations (full or circles). Parameters are the same as in Fig. 2.

expensive to converge results at large $\lambda$ thus we only show few data points in Figs. 5(d) and 6(d).

In Fig. 5, we show contour plots obtained from the exact solution, $\mathcal{N}_{\mathrm{BLP,EX}}$, in Fig. 5(a), and the RC method, $\mathcal{N}_{\mathrm{BLP,RC}}$, in Fig. 5(b). We note on the excellent agreement between the maps. As an example, we plot in Fig. 5(c) the BLP measure as a function of $\gamma$ at small coupling, observing its monotonic decay with increased $\gamma$. This is to be expected, as sharply peaked spectral functions are usually associated with a longer memory time for the system, which in turn leads to non-Markovianity. Following this, in Fig. 5(d) we study the behavior of the BLP measure with $\lambda$ for a narrow spectral function, pushing $\lambda$ to large values beyond what is included in the contour map. Here, we observe a nonmonotonic behavior: The BLP measure first rises with $\lambda$ at weak coupling, then it rapidly decays at large $\lambda$.

We examine non-Markovianity with the RHP measure in Fig. 6, again as a function of the system-bath coupling $\lambda$ and bath width parameter $\gamma$. The comparison of contour maps generated from the exact solution [Fig. 6(a)] and the RC-QME method [Fig. 6(b)] confirms that the RC method correctly captures non-Markovianity as measured by the RHP method. We display the $\gamma$ dependence in Fig. 6(c), and the $\lambda$ dependence in Fig. 6(d). In contrast to the BLP measure, the RHP metric quickly increases at large coupling without showing a turnover behavior. These contrasting trends were also observed and discussed in Refs. [37,38].

Altogether, our main observations are (i) The RC-QME method *quantitatively* captures non-Markovianity in the dynamics, including nontrivial trends as displayed in Fig. 5(d). (ii) The RC-QME may overestimate the extent of non-Markovianity in the dynamics, presumably due to the emphasis of a single-collective bath degree of freedom in the system's dynamics.

## VI. DISCUSSION AND SUMMARY

In this work, we addressed the potential of the reaction-coordinate QME method in capturing non-Markovian dynamics. The advantage of the RC-QME method in this respect is that, by adding a collective bath mode to the system, one explicitly captures its dynamics, including correlations that develop in time between the bath with system's degrees of freedom.

As a benchmark, we used the exactly solvable model of pure decoherence in a single qubit. By observing the dynamics and quantifying it with two different measures for non-Markovianity, we showed that the RC-QME method excellently captured such effects in the difficult parameter regimes of strong system-bath coupling (large $\lambda$) and highly structured baths (small $\gamma$).

We used two measures for non-Markovianity, the BLP, which tests states' distinguishability, and the RHP, which inquires on the CP-divisibility of the dynamical map. Both measures indicate that non-Markovian effects are enhanced as we reduce the width of the spectral function of the bath. This result, observed with exact expressions, agrees with common knowledge.

What is important to note is that, very favorably, the RC method becomes *more accurate* for highly structured baths. This is because this scenario precisely fits the principles of the RC mapping, of extracting a prominent-collective degree of freedom from the bath and adding it to the system. The capability of the RC-QME method to describe non-Markovian effects is particularly notable since powerful numerically exact techniques such as influence functional path integral methods [54–58] face challenges converging for narrow spectral functions.

As for strong-coupling effects, we found that the RC-QME becomes increasingly difficult to converge as we increase $\lambda$, posing a challenge in computations. Nevertheless, with increased computational work we found that the RC-QME method accurately described non-Markovian effects even in the strong-coupling limit.

The RC mapping as described in this work was done analytically with the conversion of a Brownian spectral function to an Ohmic one. While the Brownian model, and the related Debye model had found applications such as in studies of exciton dynamics in the Fenna-Matthews-Olson complex [59], it is important to remember that the RC mapping can be performed numerically on more general spectral functions, as well as iteratively, to continue and extract primary modes from the bath [10].

With the goal to gauge non-Markovian effects in the RC-QME method, we focused our efforts here on the exactly solvable pure decoherence model, Eq. (1). It is interesting to extend our analysis and examine other open quantum system models, such as the more complex spin-boson (SB) model, $\hat{H} = \frac{\Delta}{2}\hat{\sigma}_z + \hat{\sigma}_x \sum_k f_k(\hat{c}_k^\dagger + \hat{c}_k) + \sum_k \nu_k \hat{c}_k^\dagger \hat{c}_k$. Unlike the pure decoherence model, this model displays both decoherence and energy relaxation dynamics.

The dynamics of the SB model was examined in many works with a range of techniques [2]. Particularly, it was simulated in Ref. [15] by benchmarking the RC-QME method to numerically exact simulations, manifesting an excellent agreement even at strong coupling. Quantifying non-Markovian dynamics in the SB dynamics (or other nonintegrable models) based on the BLP and the RHP measures, or others, is a highly nontrivial task, given that the model does not have a closed-form solution and that it is challenging to simulate it in a numerically exact manner. Simulations of the trace-distance were performed, e.g., in Ref. [60] based on a real-time path integral method and more recently in Ref. [61] using the multilayer multiconfiguration time-dependent Hartree approach (ML-MCTDH). Perturbative approaches for dynamics were employed, e.g., in Refs. [62–65].

Given the complexity of the problem, we now simply demonstrate with the RC-QME method that the SB model at small $\gamma$ shows recoherence dynamics, see Figs. 7(c) and 7(d). These recoherences do not show up with the BMR-QME method, which is Markovian by construction. As such, we argue that these features indicate on non-Markovian dynamics. We reiterate that the RC-QME method should be quite accurate in the small-$\gamma$ regime, and even at strong coupling [15]. More details on the SB model and the corresponding dynamics of spin polarization are discussed in Appendix C.

Future work will be dedicated to capturing and quantifying strong coupling and non-Markovian effects with the RC-QME

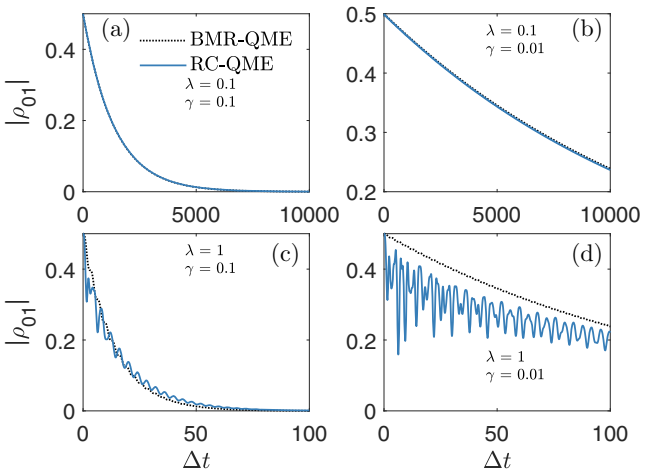


FIG. 7. Coherence dynamics of the spin-boson model for the initial state $\rho = |-\rangle\langle -|$ with $|-\rangle = (|0\rangle - |1\rangle)/\sqrt{2}$. Calculations were done with the Born-Markov Redfield equation (dotted line) and the RC-QME method (full), for details see Appendix C. Parameters are the same as in Fig. 2.

in different open quantum system models. For example, the equilibrium behavior of the V-model was recently examined in Refs. [66,67] at weak—and ultrastrong—coupling. It remains an open topic to explore the dissipative dynamics of such multilevel models at intermediate and strong coupling.

Proposals for novel quantum devices rely on nontrivial aspects of small, quantum systems [68]. Specifically, strong system-bath couplings and bath structuring are suggested as means to realize new effects. The RC-QME method has been proving itself as a powerful tool in this respect. It nicely complements numerically exact approaches, which typically struggle to converge in regimes that are favorable for RC-QME simulations. Ongoing work is focused on studies of quantum thermal machines beyond weak system-bath coupling, towards the discovery of their unique performance [69].

## ACKNOWLEDGMENTS

D.S. acknowledges support from an NSERC Discovery Grant and the Canada Research Chair program.

## APPENDIX A: MARKOVIAN LIMIT OF THE PURE DECOHERENCE MODEL

In this Appendix, we derive an expression for the decoherence timescale $\tau_D$ in the pure decoherence model. We perform our analysis on the model in its original representation, Eq. (1), using the Brownian spectral function for the bath, Eq. (2).

First, we derive the decoherence timescale by simplifying the exact analytic expression. Next, we show that one can reach the same result from the Redfield equation of motion, a method that relies on the Born-Markov approximation.

### 1. Derivation based on the exact analytic expression

We study the long-time limit of the decoherence function [3],

$$\Gamma(t) = -4\int_0^\infty d\omega J(\omega)\coth\left(\frac{\beta\omega}{2}\right)\frac{1-\cos(\omega t)}{\omega^2}. \quad \text{(A1)}$$

Unlike textbook calculations, which simplify this function assuming an Ohmic spectral function [3], here we use a Brownian spectral function for the bath,

$$J(\omega) = \frac{4\omega\Omega^2\lambda^2\gamma/\pi}{(\omega^2-\Omega^2)^2 + (2\gamma\Omega\omega)^2}. \quad \text{(A2)}$$

Noting that $1-\cos(\omega t) = 2\sin^2(\frac{\omega t}{2})$ and that, in the long-time limit, $\frac{4\sin^2(\frac{\omega t}{2})}{\omega^2} \to 2\pi t\delta(\omega)$, we get

$$\Gamma(t) \to -2\pi t\left[J(\omega)\coth\left(\frac{\beta\omega}{2}\right)\right]\Bigg|_{\omega\to 0}. \quad \text{(A3)}$$

For nonzero temperatures, $[J(\omega)\coth(\frac{\beta\omega}{2})]|_{\omega\to 0} \to \frac{8\gamma\lambda^2}{\pi\Omega^2\beta}$, thus we obtain in the long-time limit,

$$\Gamma(t) = -\frac{16\gamma\lambda^2}{\Omega^2\beta}t. \quad \text{(A4)}$$

According to this result, coherences decay exponentially in time with the decoherence timescale

$$\tau_D = \frac{\Omega^2\beta}{16\gamma\lambda^2}. \quad \text{(A5)}$$

We can now be precise and note that the "long-time limit" corresponds to $t \gg \tau_D$. Thus, the exponential form is arrived at more quickly as we increase the temperature and the coupling strength $\lambda$.

### 2. Derivation from the Born-Markov Redfield equation

In the Schrödinger representation, the Redfield QME is given by

$$\begin{aligned}\dot\rho(t) = &-i[\hat H_S, \rho(t)]\\ &-\int_0^\infty d\tau\{[\hat S, e^{-i\hat H_S\tau}\hat S e^{i\hat H_S\tau}\rho(t)]\langle\hat B(t)\hat B(t-\tau)\rangle\\ &-[\hat S, \rho(t)e^{-i\hat H_S\tau}\hat S e^{i\hat H_S\tau}]\langle\hat B(t-\tau)\hat B(t)\rangle\}. \quad \text{(A6)}\end{aligned}$$

Here, $\hat S$ is a system operator that couples to the bath operator, $\hat B$, with $\hat B(t)$ an interaction representation operator. Here, averages $\langle\hat B(t)\hat B(0)\rangle$ are calculated with respect to the thermal state of the bath (before the RC mapping). In our model, the system's Hamiltonian is $\hat H_S = \frac{\Delta}{2}\hat\sigma_z$ and $\hat S = \hat\sigma_z$; $\hat\sigma_z = |0\rangle\langle 0| - |1\rangle\langle 1|$. Since we are interested in the dynamics of coherences, we focus on the matrix element $\rho_{01}(t) = \langle 0|\rho(t)|1\rangle$. The above expression simplifies to

$$\dot\rho_{01}(t) = -i\Delta\rho_{01}(t) - 2\rho_{01}(t)\int_{-\infty}^\infty d\tau\langle\hat B(\tau)\hat B(0)\rangle, \quad \text{(A7)}$$

where we assumed that the bath is stationary thus $\langle\hat B(0)\hat B(\tau)\rangle = \langle\hat B(-\tau)\hat B(0)\rangle$, allowing us to combine two bath correlation functions into a single integral. To compute the bath correlation function we note that

$\hat{B}(\tau) = \sum_k f_k(\hat{b}_k e^{-i\nu_k\tau} + \hat{b}_k^\dagger e^{i\nu_k\tau})$. Using this and moving to the continuum limit we get

$$\langle \hat{B}(\tau)\hat{B}(0)\rangle = \int_0^\infty d\omega J(\omega)\{[1+n_{\rm B}(\omega)]e^{-i\omega\tau} + n_{\rm B}(\omega)e^{i\omega\tau}\}, \tag{A8}$$

with $n_{\rm B}(\omega) = (e^{\beta\omega}-1)^{-1}$ being the Bose-Einstein distribution function. It is now possible to perform the time integral in Eq. (A7) using $2\pi\delta(\omega) = \int_{-\infty}^{\infty} d\tau e^{i\omega\tau}$,

$$\dot{\rho}_{01}(t) = -i\Delta\rho_{01}(t) - 4\pi\rho_{01}(t)\int_0^\infty d\omega J(\omega)[2n_{\rm B}(\omega)+1]\delta(\omega). \tag{A9}$$

Evaluating the trivial integral we get

$$\dot{\rho}_{01}(t) = -i\Delta\rho_{01}(t) - 2\pi J(0)[2n_{\rm B}(0)+1]\rho_{01}(t). \tag{A10}$$

Care needs to be taken when evaluating the second term as $n_{\rm B}(0)$ is divergent. To keep the discussion general for now we define $A \equiv 2\pi \lim_{\omega\to 0} J(\omega)[2n_{\rm B}(\omega)+1]$, assuming this expression has a well-defined limit. The inverse of this term corresponds to the decoherence timescale, $\tau_D = A^{-1}$. Altogether, the differential equation (A10) solves to

$$\rho_{01}(t) = \rho_{01}(0)e^{-i\Delta t}e^{-At}. \tag{A11}$$

As expected, the Born-Markov approximation results in an exponentially decaying dynamics for $\rho_{01}$. Coherences are affected by two timescales. While $\Delta^{-1}$ is related to intrinsic coherent oscillations, $\tau_D$ describes the loss of coherence with time due to the coupling to the bath. We can now explicitly evaluate this latter timescale using the Brownian spectral function, resulting in $\tau_D = \frac{\beta\Omega^2}{16\gamma\lambda^2}$, which agrees with results from Sec. 1 of this Appendix.

## APPENDIX B: DETAILS OF THE REDFIELD EQUATION

For completeness, we provide here the full reaction-coordinate Redfield equation that we use in the main text to simulate the dynamics of the supersystem. Working in the Schrödinger picture and in the energy-basis of the subsystem, the Redfield equation for the reduced density matrix of the supersystem (dimension $2M$) is given by

$$\begin{aligned}\dot{\rho}_{{\rm ES},mn}(t) &= -i\omega_{mn}\rho_{{\rm ES},mn}(t) \\ &- \sum_{j,k}[R_{mj,jk}(\omega_{kj})\rho_{{\rm ES},kn}(t) + R^*_{nk,kj}(\omega_{jk})\rho_{{\rm ES},mj}(t) \\ &- R_{kn,mj}(\omega_{jm})\rho_{{\rm ES},jk}(t) - R^*_{jm,nk}(\omega_{kn})\rho_{{\rm ES},jk}(t)].\end{aligned} \tag{B1}$$

Here $\omega_{mn} = \omega_m - \omega_n$ are Bohr frequencies of the extended system. The dissipator itself is given by half Fourier transforms of the bath autocorrelation function,

$$\begin{aligned}R_{mn,jk}(\omega) &= \left(S^D_{\rm ES}\right)_{mn}\left(S^D_{\rm ES}\right)_{jk}\int_0^\infty d\tau e^{i\omega\tau}\langle\hat{B}(\tau)\hat{B}(0)\rangle \\ &= \left(S^D_{\rm ES}\right)_{mn}\left(S^D_{\rm ES}\right)_{jk}[\Gamma_{\rm RC}(\omega) + i\Delta_{\rm RC}(\omega)].\end{aligned} \tag{B2}$$

Averages $\langle\hat{B}(t)\hat{B}(0)\rangle$ are calculated with respect to the thermal state of the *residual* bath, $\rho_B = e^{-\beta\hat{H}_B}/{\rm Tr}[e^{-\beta\hat{H}_B}]$. In simulations, we neglect the imaginary part of the Redfield tensor, $\Delta_{\rm RC}(\omega)$. Detailed discussions about the role of this self-energy in the steady-state limit for specialized models (beyond the decoherence model and the spin-boson model discussed in this work) appear in Refs. [67,70]. The real portion of the correlation function can be readily evaluated to yield

$$\Gamma_{\rm RC}(\omega) = \begin{cases}\pi J_{\rm RC}(\omega)n(\omega) & \omega > 0 \\ \pi J_{\rm RC}(|\omega|)[(n(|\omega|)+1] & \omega < 0 \\ \gamma/\beta & \omega = 0 \quad \text{(Ohmic model)}.\end{cases} \tag{B3}$$

$n(\omega)$ is the Bose-Einstein distribution function and $J_{\rm RC}(\omega)$ is the spectral function of the residual bath given by Eq. (6).

## APPENDIX C: NON-MARKOVIAN EFFECTS IN THE SPIN-BOSON MODEL

The decoherence model, Eq. (1), does not allow dissipative (energy exchange) dynamics. In contrast, the spin-boson model

$$\hat{H} = \frac{\Delta}{2}\hat{\sigma}_z + \hat{\sigma}_x\sum_k f_k(\hat{c}_k^\dagger + \hat{c}_k) + \sum_k \nu_k\hat{c}_k^\dagger\hat{c}_k \tag{C1}$$

displays more complex dissipative and decoherence dynamics. Similarly to Eq. (1), $\Delta$ is the spin splitting, $\hat{\sigma}_z = |0\rangle\langle 0| - |1\rangle\langle 1|$, $\hat{\sigma}_x = |1\rangle\langle 0| + |0\rangle\langle 1|$, $\hat{c}_k^\dagger$ ($\hat{c}_k$) are bosonic creation (annihilation) operators for mode $k$, with $f_k$ a coupling energy. While the dynamics of the SB model can be analytically described in different limits [2], a complete, exact analytic solution is unavailable.

Applying the reaction coordinate mapping to the spin-boson model (C1), we get the following Hamiltonian:

$$\begin{aligned}\hat{H}_{\rm RC} &= \frac{\Delta}{2}\hat{\sigma}_z + \lambda\hat{\sigma}_x(\hat{a}^\dagger + \hat{a}) + \Omega\hat{a}^\dagger\hat{a} + (\hat{a}^\dagger + \hat{a})^2\sum_k\frac{g_k^2}{\omega_k} \\ &+ (\hat{a}^\dagger + \hat{a})\sum_k g_k(\hat{b}_k^\dagger + \hat{b}_k) + \sum_k \omega_k\hat{b}_k^\dagger\hat{b}_k.\end{aligned} \tag{C2}$$

The original model takes a Brownian spectral function for the bath. After the RC mapping, the residual bath is coupled (presumably) weakly to the system with an Ohmic spectral function.

We now focus on the appearance of non-Markovian dynamics as we reduce $\gamma$ and increase $\lambda$. Since quantifying non-Markovian dynamics using the BLP and RHP measures is nontrivial for the spin-boson model, we only examine this concept qualitatively by comparing the RC-QME results to Markovian simulations. The dynamics of coherences in the spin-boson model is displayed in the main text, Fig. 7. There,

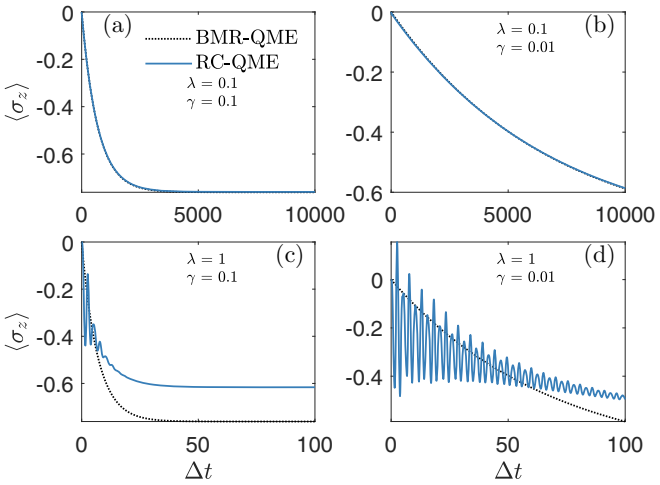


FIG. 8. Polarization dynamics in the spin-boson model, $\langle\sigma_z(t)\rangle$, with the initial state $\rho = |-\rangle\langle -|$ using the BMR-QME method (dotted line) and the RC-QME method (full line). Parameters are the same as in Fig. 2.

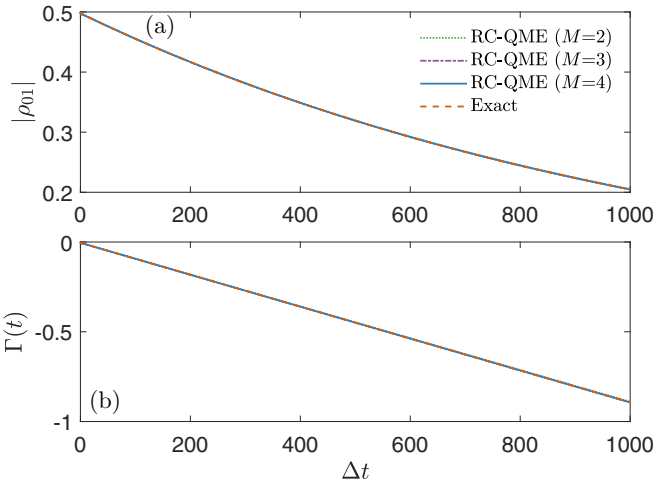


FIG. 9. Convergence of RC-QME simulations, Fig. 2(a), with respect to $M$ at weak coupling, $\lambda = 0.1$. We present (a) the decoherence dynamics and (b) corresponding decoherence function for $M = 2$ (dotted), 3 (dashed-dotted), 4 (full), and compare those with exact results (dashed). Parameters are $\lambda = 0.1$ and $\gamma = 0.1$, as well as $\Delta = 1$, $\Omega = 3\Delta$, $T = 0.5\Delta$, $\Lambda = 1000\pi\,\Delta$, as in Fig. 2(a).

we show that as we increase the coupling strength and reduce $\gamma$ we see pronounced deviations from Markovian dynamics, captured by the RC method. The corresponding dynamics of polarization is depicted in Fig. 8. We find that the BMR-QME method misses the damped coherent oscillations in the dynamics that show up at strong coupling and small $\gamma$. Furthermore, the BMR-QME method no longer provides the correct long-time solution at strong coupling.

The RC-QME method predicts significant deviations from Markovian dynamics in the spin-boson model once we structure the bath and enhance coupling strength. Benchmarking RC-QME results at small $\gamma$ against numerically exact simulations is challenging: For example, consider the quasi-adiabatic propagator path integral (QuAPI) method [54,55]: For $\gamma = 0.01$ and $\Omega = 3$, the bath memory time may be approximated by $\tau_M \sim 1/(\gamma\Omega) \approx 30$. To properly capture the damped coherent oscillations (of period $2\pi/\Delta$), and reduce the Trotter error, one needs to adopt a short time step of $\delta t \approx 0.2$. Thus, to cover the memory time one needs a memory kernel with $N \sim \tau_M/\delta t \approx 200$ segments. This significant task may be achieved with advanced implementations of numerically exact path integral approaches [56–58], and we leave it to future work.

## APPENDIX D: ADDITIONAL CONVERGENCE RESULTS

The computational complexity of the RC-QME method scales as $O((d\times M)^4)$ due to the need to construct the Redfield tensor for the $(dM)\times(dM)$ reduced density matrix. Here, $d$ is the dimension of the original subsystem (2 for spin) and $M$ the number of truncated levels in the RC.

In this Appendix, we present additional $M$-convergence results, analogous to Fig. 4. There, we focused on the challenge in converging coherences once the system-bath coupling strength was made large, $\lambda > \Omega$. In contrast, here in Figs. 9 and 10 we show that in both weak and intermediate couplings, $\lambda < \Omega$, convergence is simple, pointing to the utility of the RC-QME method.

First, at weak coupling we show in Fig. 9 that even just including $M = 2$ levels in the RC is already sufficient for results to be converged. The intermediate coupling regime is presented in Fig. 10; here convergence with respect to $M$ is reached at $M = 5$, which is still a simple computational task. Altogether, we emphasize that ensuring convergence with respect to $M$ is a critical aspect of the RC-QME technique. In the pure-decoherence model presented in this study convergence poses a technical challenge only in the strong-coupling regime.

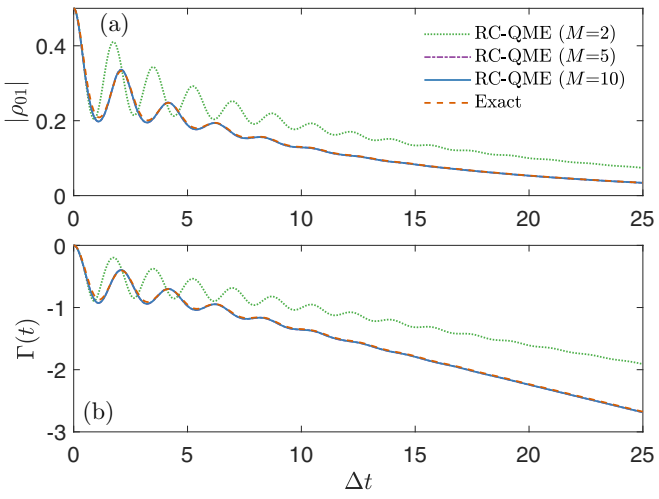


FIG. 10. Convergence of RC-QME simulations, Fig. 2(c), with respect to $M$ at intermediate coupling, $\lambda = 1$. We present (a) the decoherence dynamics and (b) corresponding decoherence function for $M = 2$ (dotted), 5 (dashed-dotted), 10 (full), and compare those to exact results (dashed). Parameters are $\lambda = 1$ and $\gamma = 0.1$ as well as $\Delta = 1$, $\Omega = 3\Delta$, $T = 0.5\Delta$, $\Lambda = 1000\pi\,\Delta$ as in Fig. 2(c).

[1] A. Nitzan, *Chemical Dynamics in Condensed Phases: Relaxation, Transfer and Reactions in Condensed Molecular Systems* (Oxford University Press, Oxford, UK, 2006).

[2] U. Weiss, *Quantum Dissipative Systems* (World Scientific, Singapore, 2012).

[3] H. P. Breuer and F. Petruccione, *The Theory of Open Quantum Systems* (Oxford University Press, Oxford, 2007).

[4] D. A. Lidar, Lecture notes on the theory of open quantum systems, arXiv:1902.00967.

[5] A. Rivas, S. F. Huelga, and M. B. Plenio, Quantum non-Markovianity: Characterization, quantification and detection, Rep. Prog. Phys. **77**, 094001 (2014).

[6] L. Li, M. J. W. Hall, and H. W. Wiseman, Concepts of quantum non-Markovianity: A hierarchy, Phys. Rep. **759**, 1 (2018).

[7] H.-P. Breuer, Foundations and measures of quantum non-Markovianity, J. Phys. B: At. Mol. Opt. Phys. **45**, 154001 (2012).

[8] I. de Vega and D. Alonso, Dynamics of non-Markovian open quantum systems, Rev. Mod. Phys. **89**, 015001 (2017).

[9] C.-F. Li, G.-C. Guo, and J. Piilo, Non-Markovian quantum dynamics: What does it mean? Europhys. Lett. **127**, 50001 (2019).

[10] A. Nazir and G. Schaller, The reaction coordinate mapping in quantum thermodynamics, in *Thermodynamics in the Quantum Regime: Fundamental Aspects and New Directions* (Springer International Publishing, Cham, 2018), pp. 441–577.

[11] K. H. Hughes, C. D. Christ, and I. Burghardt, Effective-mode representation of non-Markovian dynamics: A hierarchical approximation of the spectral density. I. Application to single surface dynamics, J. Chem. Phys. **131**, 024109 (2009).

[12] K. H. Hughes, C. D. Christ, and I. Burghardt, Effective-mode representation of non-Markovian dynamics: A hierarchical approximation of the spectral density. II. Application to environment-induced nonadiabatic dynamics, J. Chem. Phys. **131**, 124108 (2009).

[13] R. Martinazzo, B. Vacchini, K. H. Hughes, and I. Burghardt, Universal Markovian reduction of Brownian particle dynamics, J. Chem. Phys. **134**, 011101 (2011).

[14] J. Iles-Smith, N. Lambert, and A. Nazir, Environmental dynamics, correlations, and the emergence of noncanonical equilibrium states in open quantum systems, Phys. Rev. A **90**, 032114 (2014).

[15] J. Iles-Smith, A. G. Dijkstra, N. Lambert, and A. Nazir, Energy transfer in structured and unstructured environments: Master equations beyond the Born-Markov approximations, J. Chem. Phys. **144**, 044110 (2016).

[16] C. L. Latune, Steady state in strong bath coupling: reaction coordinate versus perturbative expansion, arXiv:2110.03169.

[17] L. A. Correa, B. Xu, B. Morris, and G. Adesso, Pushing the limits of the reaction-coordinate mapping, J. Chem. Phys. **151**, 094107 (2019).

[18] N. Anto-Sztrikacs and D. Segal, Strong coupling effects in quantum thermal transport with the reaction coordinate method, New J. Phys. **23**, 063036 (2021).

[19] P. Strasberg, G. Schaller, N. Lambert, and T. Brandes, Nonequilibrium thermodynamics in the strong coupling and non-Markovian regime based on a reaction coordinate mapping, New J. Phys. **18**, 073007 (2016).

[20] D. Newman, F. Mintert, and A. Nazir, Performance of a quantum heat engine at strong reservoir coupling, Phys. Rev. E **95**, 032139 (2017).

[21] D. Newman, F. Mintert, and A. Nazir, Quantum limit to nonequilibrium heat-engine performance imposed by strong system-reservoir coupling, Phys. Rev. E **101**, 052129 (2020).

[22] P. Strasberg, G. Schaller, T. L. Schmidt, and M. Esposito, Fermionic reaction coordinates and their application to an autonomous Maxwell demon in the strong-coupling regime, Phys. Rev. B **97**, 205405 (2018).

[23] S. Restrepo, S. Böhling, J. Cerrillo, and G. Schaller, Electron pumping in the strong coupling and non-Markovian regime: A reaction coordinate mapping approach, Phys. Rev. B **100**, 035109 (2019).

[24] C. McConnell and A. Nazir, Strong coupling in thermoelectric nanojunctions: A reaction coordinate framework, arXiv:2106.14799.

[25] S. A. Adelman and J. D. Doll, Generalized Langevin equation approach for atom/solid–surface scattering: General formulation for classical scattering off harmonic solids, J. Chem. Phys. **64**, 2375 (1976).

[26] Y. Tanimura and P. G. Wolynes, Quantum and classical Fokker-Planck equations for a Gaussian-Markovian noise bath, Phys. Rev. A **43**, 4131 (1991).

[27] B. M. Garraway, Decay of an atom coupled strongly to a reservoir, Phys. Rev. A **55**, 4636 (1997).

[28] C. Meier and D. J. Tannor, Non-Markovian evolution of the density operator in the presence of strong laser fields, J. Chem. Phys. **111**, 3365 (1999).

[29] D. Tamascelli, A. Smirne, J. Lim, S. F. Huelga, and M. B. Plenio, Efficient Simulation of Finite-Temperature Open Quantum Systems, Phys. Rev. Lett. **123**, 090402 (2019).

[30] T. Chen, V. Balachandran, C. Guo, and D. Poletti, Steady-state quantum transport through an anharmonic oscillator strongly coupled to two heat reservoirs, Phys. Rev. E **102**, 012155 (2020).

[31] A. Rivas, S. F. Huelga, and M. B. Plenio, Entanglement and Non-Markovianity of Quantum Evolutions, Phys. Rev. Lett. **105**, 050403 (2010).

[32] H.-P. Breuer, E.-M. Laine, and J. Piilo, Measure for the Degree of Non-Markovian Behavior of Quantum Processes in Open Systems, Phys. Rev. Lett. **103**, 210401 (2009).

[33] X.-M. Lu, X. Wang, and C. P. Sun, Quantum Fisher information flow and non-Markovian processes of open systems, Phys. Rev. A **82**, 042103 (2010).

[34] S. Luo, S. Fu, and H. Song, Quantifying non-Markovianity via correlations, Phys. Rev. A **86**, 044101 (2012).

[35] F. F. Fanchini, G. Karpat, B. Cakmak, L. K. Castelano, G. H. Aguilar, O. J. Farias, S. P. Walborn, P. H. Ribeiro, and M. C. de Oliveira, Non-Markovianity through Accessible Information, Phys. Rev. Lett. **112**, 210402 (2014).

[36] S. Lorenzo, F. Plastina, and M. Paternostro, Geometrical characterization of non-Markovianity, Phys. Rev. A **88**, 020102(R) (2013).

[37] C. Addis, B. Bylicka, D. Chruściński, and S. Maniscalco, Comparative study of non-Markovianity measures in exactly solvable one- and two-qubit models, Phys. Rev. A **90**, 052103 (2014).

[38] G. Guarnieri, A. Smirne, and B. Vacchini, Quantum regression theorem and non-Markovianity of quantum dynamics, Phys. Rev. A **90**, 022110 (2014).

[39] Z. He, J. Zou, L. Li, and B. Shao, Effective method of calculating the non-Markovianity $\mathcal{N}$ for single-channel open systems, Phys. Rev. A **83**, 012108 (2011).
[40] F. F. Fanchini, G. Karpat, D. Z. Rossatto, A. Norambuena, and R. Coto, Estimating the degree of non-Markovianity using machine learning, Phys. Rev. A **103**, 022425 (2021).
[41] Z. He, H.-S. Zeng, Y. Chen, and C. Yao, Non-Markovian dynamics of a dephasing model in a squeezed thermal bath, Laser Phys. Lett. **16**, 065204 (2019).
[42] H. Z. Shen, D. X. Li, Shi-Lei Su, Y. H. Zhou, and X. X. Yi, Exact non-Markovian dynamics of qubits coupled to two interacting environments, Phys. Rev. A **96**, 033805 (2017).
[43] W. H. Zurek, Decoherence, einselection, and the quantum origins of the classical, Rev. Mod. Phys. **75**, 715 (2003).
[44] P. W. Shor, Scheme for reducing decoherence in quantum computer memory, Phys. Rev. A **52**, R2493(R) (1995).
[45] L. Ratschbacher, C. Sias, L. Carcagni, J. M. Silver, C. Zipkes, and M. Köhl, Decoherence of a Single-Ion Qubit Immersed in a Spin-Polarized Atomic Bath, Phys. Rev. Lett. **110**, 160402 (2013).
[46] D. Khurana, B. K. Agarwalla, and T. S. Mahesh, Experimental emulation of quantum non-Markovian dynamics and coherence protection in the presence of information backflow, Phys. Rev. A **99**, 022107 (2019).
[47] Z. D. Liu, H. Lyyra, Y. N. Sun, B. H. Liu, C. F. Li, G. C. Guo, S. Maniscalco, J. Piilo *et al.*, Experimental implementation of fully controlled dephasing dynamics and synthetic spectral densities, Nat. Commun. **9**, 3453 (2018).
[48] M. T. Mitchison, A. Purkayastha, M. Brenes, A. Silva, and J. Goold, Taking the temperature of a pure quantum state, arXiv:2103.16601.
[49] M. Kilgour (private communication), https://hdl.handle.net/1807/97509
[50] M. Popovic, M. T. Mitchison, and J. Goold, Thermodynamics of decoherence, arXiv:2107.14216.
[51] The form of the spectral density function here differs from the convention set in Ref. [18] by a factor of $\pi$.
[52] S. Garmon, T. Petrosky, L. Simine, and D. Segal, Amplification of non-Markovian decay due to bound state absorption into continuum, Fortschr. Phys. **61**, 261 (2013).
[53] S. Garmon, K. Noba, G. Ordonez, and D. Segal, Non-Markovian dynamics revealed at a bound state in the continuum, Phys. Rev. A **99**, 010102(R) (2019).
[54] N. Makri and D. E. Makarov, Tensor propagator for iterative quantum time evolution of reduced density matrices. I. Theory, J. Chem. Phys. **102**, 4600 (1995).
[55] N. Makri and D. E. Makarov, Tensor propagator for iterative quantum time evolution of reduced density matrices. II. Numerical methodology, J. Chem. Phys. **102**, 4611 (1995).
[56] N. Makri, Small matrix disentanglement of the path integral: Overcoming the exponential tensor scaling with memory length, J. Chem. Phys. **152**, 041104 (2020).
[57] N. Makri, Small matrix path integral for system-bath dynamics, J. Chem. Theory Comput. **16**, 4038 (2020).
[58] A. Strathearn, P. Kirton, D. Kilda, J. Keeling, and B. W. Lovett, Efficient non-Markovian quantum dynamics using time-evolving matrix product operators, Nat. Commun. **9**, 1 (2018).
[59] P. Nalbach, D. Braun, and M. Thorwart, Exciton transfer dynamics and quantumness of energy transfer in the Fenna-Matthews-Olson complex, Phys. Rev. E **84**, 041926 (2011).
[60] C. A. Mujica-Martinez, P. Nalbach, and M. Thorwart, Quantification of non-Markovian effects in the Fenna-Matthews-Olson complex, Phys. Rev. E **88**, 062719 (2013).
[61] S. Wenderoth, H.-P. Breuer, and M. Thoss, Non-Markovian effects in the spin-boson model at zero temperature, Phys. Rev. A **104**, 012213 (2021).
[62] G. Clos and H.-P. Breuer, Quantification of memory effects in the spin-boson model, Phys. Rev. A **86**, 012115 (2012).
[63] H.-B. Chen, N. Lambert, Y.-C. Cheng, Y.-N. Chen, and F. Nori, Using non-Markovian measures to evaluate quantum master equations for photosynthesis, Sci. Rep. **5**, 12753 (2015).
[64] A. Rivas, Refined weak-coupling limit: Coherence, entanglement, and non-Markovianity, Phys. Rev. A **95**, 042104 (2017).
[65] M. Hinarejos, M.-C. Banuls, A. Perez, and I. de Vega, Non-Markovianity and memory of the initial state, J. Phys. A: Math. Theor. **50**, 335301 (2017).
[66] A. Dodin and P. Brumer, Noise-Induced Coherence in Molecular Processes, arXiv:2109.06803.
[67] J. D. Cresser and J. Anders, Weak and ultrastrong coupling limits of the quantum mean force Gibbs state, arXiv:2104.12606.
[68] S. Vinjanampathy and J. Anders, Quantum thermodynamics, Contemp. Phys. **57**, 545 (2016).
[69] F. Ivander, N. Anto-Sztrikacs, and D. Segal, Strong system-bath coupling reshapes characteristics of quantum thermal machines, arXiv:2111.05302.
[70] A. Purkayastha, G. Guarnieri, M. T. Mitchison, R. Filip, and J. Goold, Tunable phonon-induced steady state coherence in a double-quantum-dot charge qubit, npj Quantum Inf. **6**, 27 (2020).